Available online at www.sciencedirect.com
ScienceDirect
Proceedings of the Combustion Institute 33 (2011) 577–584
Proceedings of the Combustion Institute
www.elsevier.com/locate/proci

Soot formation in laminar ethane diffusion flames at pressures from 0.2 to 3.3 MPa

Paul M. Mandatori, Ömer L. Gülder *

Institute for Aerospace Studies, University of Toronto, 4925 Dufferin Street, Toronto, Ontario, Canada M3H 5T6

Available online 9 August 2010

Abstract

The effects of pressure on soot formation and the structure of the temperature field were studied in co-flow ethane-air laminar diffusion flames over the pressure range of 0.1–3.34 MPa in a high pressure combustion chamber. The selected fuel mass flow rate provided diffusion flames in which the soot was completely oxidized within the visible flame envelope and the flame was stable at all pressures considered. The spatially resolved soot volume fraction and soot temperature were measured by spectral soot emission as a function of pressure. The visible (luminous) flame height remained almost unchanged from 1.52 to 3.34 MPa, whereas it increased considerably from atmospheric to 1.52 MPa. Flame cross-sectional area, measured at the flame height of 5 mm either bounded by maximum flame temperature or maximum soot volume fraction contours, showed an inverse dependence on pressure. Peak carbon conversion to soot, defined as the percentage of fuel's carbon content converted to soot, showed a strong dependence on pressure at lower pressures; but this dependence grew weaker as the pressure was increased. This dependence can be expressed as a pressure scaling in the form of a power law. However, the exponent of pressure was not constant: it was about 2.2 for pressures between 0.2 and 0.51 MPa, about 1.1 for pressures between 0.51 and 1.52 MPa, and about 0.4 for pressures between 1.52 and 3.34 MPa. Averaged flame temperatures decreased with increasing pressure as a result of enhanced heat loss from the flame by soot radiation. The maximum temperature gradients increased with pressure at lower flame heights; at higher locations in the flame, after an initial increase at the lower pressure range, gradients reached a plateau at about 1.5–2.0 MPa.

Keywords: High pressure soot formation; High pressure combustion; Laminar ethane diffusion flame; Pressure dependence of soot formation; Temperature of high-pressure diffusion flames

1. Introduction

Pressure is one of the most important parameters that influence the rate of soot formation and oxidation in combustion systems. Our current understanding of pressure influence on soot formation and oxidation is limited, although most of the practical combustion devices, used in transportation systems and stationary gas turbine combustors, operate at elevated pressures.

Experimental research work related to soot formation in laminar diffusion flames at high pressures are limited to very few studies. Flower and Bowman [1] studied laminar diffusion flames of ethylene at a pressure range of 0.1–1 MPa, by

* Corresponding author. Fax: +1 416 667 7799.
E-mail address: ogulder@utias.utoronto.ca (Ö.L. Gülder).

1540-7489/$ - see front matter © 2010 The Combustion Institute. Published by Elsevier Inc. All rights reserved.
doi:10.1016/j.proci.2010.06.004

measuring line-of-sight integrated soot volume fractions and temperatures along the flame centerline. They report a pressure scaling of the maximum integrated soot volume fraction with an exponent of 1.2 ± 0.1 from atmospheric to 1 MPa pressure for ethylene diffusion flames. Measurements of Lee and Na [2] indicate a similar pressure scaling for the maximum integrated soot volume fraction with an exponent of 1.26 in laminar ethylene flames from atmospheric to 0.4 MPa. McCrain and Roberts [3] measured path integrated and local soot volume fractions by line-of-sight attenuation and laser-induced incandescence, respectively. Their measurements covered a pressure range of 0.1–2.5 MPa in methane flames and 0.1–1.6 MPa in ethylene diffusion flames. The first detailed data sets of radially resolved soot concentration and soot temperature measurements at elevated pressures up to 4 MPa were reported by Thomson et al. [4] and up to 6 MPa by Joo and Gülder [5], in laminar diffusion flames of methane using soot emission spectroscopy. Measurements by Bento et al. [6] on laminar diffusion flames of propane covered the pressure range from atmospheric to 0.73 MPa, and their results were comparable to the low pressure range reported in [4].

Ethane is not a very common fuel for combustion in pure form, but it is one of the major components in petroleum gas (as used in liquefied petroleum gas) and a pyrolysis product of hydrocarbons. Ethane is also important as an industrial feedstock for producing unique materials through partial oxidation or pyrolysis. A typical example is the production of ethylene with an annual rate of about 25 million tons in US alone [7,8] and in an amount exceeding 107 million tons worldwide in 2005 [9]. Ethane is favored for ethylene production because the steam cracking of ethane is fairly selective for ethylene.

Information on soot formation processes in laminar diffusion flames at higher pressures is limited to ethylene, methane, and propane flames [1–6,10,11]. The main objective of the research reported in this paper was to determine spatially resolved soot volume fraction and temperature in a co-flow ethane-air laminar diffusion flame at elevated pressures. Spectral soot emission measurements in the ethane flame are presented for pressures from 0.2 to 3.34 MPa. The higher pressure limit was set by the fact that ethane liquefies above this pressure. Further, it was found that at about 3.65 MPa, excessive soot formation leads to complete conversion of ethane's carbon to solid [12].

2. Experimental methodology

The experimental high pressure combustion chamber and the laminar diffusion flame burner used in this study are described in detail in [4–6]. The design pressure of the chamber is about 110 atm, and its internal diameter and internal height are 0.24 m and 0.6 m, respectively. Optical access into the chamber is through three ports at 0, 90, and 180 degree locations allowing line-of-sight measurements as well as 90° scattering and imaging experiments. The burner has a fuel nozzle exit diameter of 3.06 mm and an air nozzle diameter of 25 mm. Sintered metal foam elements inserted into the fuel and air nozzles minimize the instabilities in the flow and create a top hat exit velocity profile.

The theory and overall experimental layout of the spectral soot emission diagnostic (SSE) are described previously [4,13]. In SSE, line-of-sight radiation emission from soot is measured along chords through the flame. A series of emission projections at a given height in the flame can be inverted to obtain radially resolved emission rates from which temperature and soot volume fraction can be determined when soot optical properties are known [14]. The emitted radiation from soot first passes through an adjustable aperture and lens unit. For the current study an aperture diameter of about 6.2 mm and associated f-number of f/48 was used. The lens selected for this study is an achromatic doublet lens with a focal length of 300 mm. The lens has an antireflective coating, effective within the wavelength range of 650–1050 nm. The purpose of the lens is to image the flame radiation onto the entrance slit of the spectrometer. The lens is positioned to produce a 1:1 image. The entrance to the spectrometer contains two slits: the vertical slit is approximately 25 μm in width and the horizontal slit is approximately 290 μm in height. The slit sizes play a role in the resulting spatial resolution of the collected data.

The spectrometer is an imaging Czerny–Turner spectrometer that internally uses aspheric mirrors. The spectrometer grating used has a blaze wavelength of 775 nm and is manufactured with 300 groves/mm. The spectrometer has a dispersion of approximately 18.84 nm/mm. Soot emission is measured over a wavelength range of 690–945 nm.

The total array size of the CCD is 1340×400 pixels. However, due to the restricted size of the entrance slit, a region of interest of size 1340×80 pixels was selected. Combined with the previously mentioned spectrometer and grating, the CCD camera is capable of capturing an approximate wavelength spread of 505 nm across the camera array, providing a spectral step size of 0.377 nm/pixel. However the CCD resolution at FWHM (full width at half maximum) using 2.5 pixels, is approximately 0.942 nm.

The horizontal spatial resolution was found to be approximately 70 μm. The vertical spatial resolution was inferred to be approximately 290 μm. To calibrate the spectral axis of the CCD array a pencil style neon calibration lamp was used.

The system is calibrated for radiation intensity using a filament lamp, with a calibration traceable to NIST, placed inside the chamber. The uncertainty in the spectral radiance temperature is about 5 K. Further details of the experimental set-up and data reduction are given in [4–6].

The fuel flow rate was selected to match the carbon mass flow rate of the studies performed previously with methane diffusion flames up to 6 MPa [5], and propane diffusion flames up to 0.73 MPa [6]. A constant ethane mass flow rate of 0.52 mg/s, which corresponds to a carbon mass flow rate of 0.41 mg/s, was maintained at all pressures. For each pressure, measurements were obtained at height increments of 0.5 mm from the burner tip to the tip of the flame and at horizontal increments of 50 μm.

3. Results and discussion

3.1. Visible flame shape

Flame shape was found to change both in height, width and curvature with increasing pressure, from 0.10 to 3.34 MPa, Fig. 1. However visible flame heights, as indicated by soot radiation, remained constant at about 10 mm between pressures 1.01 and 3.34 MPa, Fig. 1. For pressures lower than 1.0 MPa, visible flame heights tended to decrease and the blue flame region near the nozzle exit became more expansive as the pressure approached atmospheric pressure. Soot formation seemed to occur mainly at the tip of the flame for lower pressures, however as the pressure increased, the luminous carbon zone moved downward filling an increasingly larger portion of the flame as also noted in the previous high pressure experiments with methane and propane [4–6].

The radial locations of the peak soot volume fractions and peak temperatures were extracted across all pressures, and the associated circular cross-sectional areas were computed at a flame height of 5 mm. As the pressure was increased, axial flame diameters decreased giving an overall stretched appearance to the flame as noted previously [1,4–6]. For pressures between 0.2 and 3.34 MPa, the flame radius varied as, $r_f \propto P^{-0.5}$ and the flame cross-sectional area varied as, $A_f \propto P^{-1}$ (Fig. 2). This observation is in agreement with previous experimental results using methane and propane flames [3,5,6]. An inverse dependence on pressure for the flame cross-sectional area implies that residence times are independent of pressure which allows measurements to be compared at the same height above the burner exit. This has also been confirmed by a recent numerical effort [15] that shows that the axial velocity profiles are pressure independent along the flame centerline in methane diffusion flames between 0.5 and 4 MPa.

3.2. Soot volume fractions

A plot that superimposes the soot volume fraction and soot temperature profiles at 0.2 MPa is shown in Fig. 3. Similar relative positions of soot and temperature peaks are observed at all pressures. It is clear that the pressure dependence of temperature profiles mirrors that of the soot profiles, Fig. 4. However the temperature profiles and the soot volume fraction profiles become radially closer to the flame centerline as the pressure is increased. This is due to the overall narrowing of the flame associated with increased pressures.

Radial soot concentration profiles in ethane diffusion flames are shown in Fig. 5 as a function of pressure and height above the burner rim. Measurements were made by scanning the entire flame diameter at each measurement height; however, the data shown in Fig. 5 represent averages of the left and right side scans. Soot forms first in an annular band near the burner rim, much like the atmospheric laminar diffusion flames. Near the mid height of the flame, the annular distribution of soot remains pronounced, but soot also begins to appear in the core of the flame. Soot appearance in the core of the flame at lower flame heights occurs at higher pressures. At the tip of

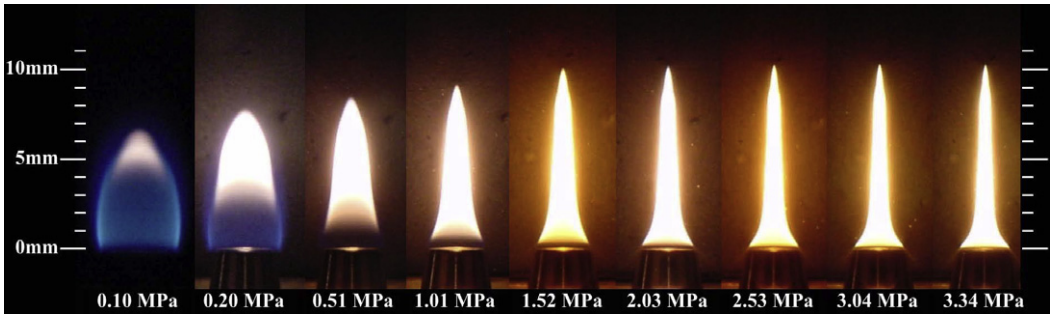

Fig. 1. Pictures of ethane diffusion flame at various pressures. Note that 0.1 MPa is about 1 atm.

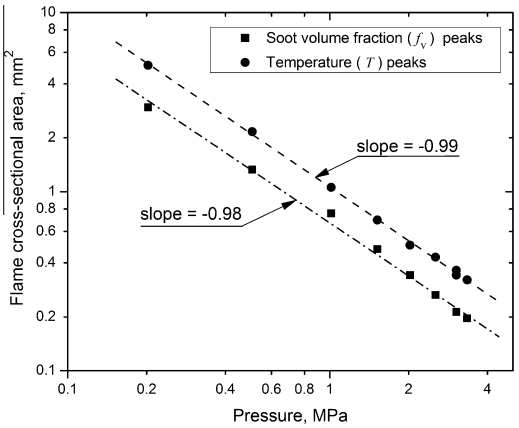

Fig. 2. Dependence of flame cross-sectional area on pressure at 5 mm flame height. Flame cross-sectional area is taken as either bounded by the maximum temperature, T, or maximum soot volume fraction, f_v, contours.

the flame, the annular distribution disappears and a peak soot concentration is observed on the flame centreline. The contraction of the flame diameter with pressure is reflected in the location of the peaks in the radial profiles of soot volume fraction. Soot concentrations showed a significant increase with pressure; the peak soot volume fraction increased from about 1.3 ppm at 0.2 MPa pressure to about 375 ppm at 3.34 MPa (Fig. 5).

As expected, soot volume fraction increases with increasing pressure since the flame is narrowing which suggests that all species are at higher concentrations. Further, the enhanced air entrainment with pressure into the flame near the burner rim is expected to accelerate the pyrolysis process [15]. To assess the sensitivity of sooting propensity of the flame to pressure, previous studies suggested [1,4–6] that the percentage of total carbon in the fuel converted to soot as a function of

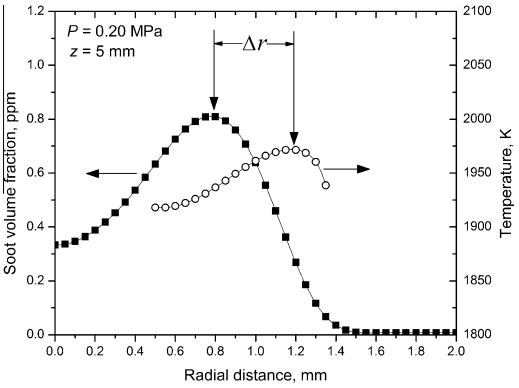

Fig. 3. Relative positions of the temperature and soot volume fraction profiles at 0.2 MPa at a flame height of 5 mm.

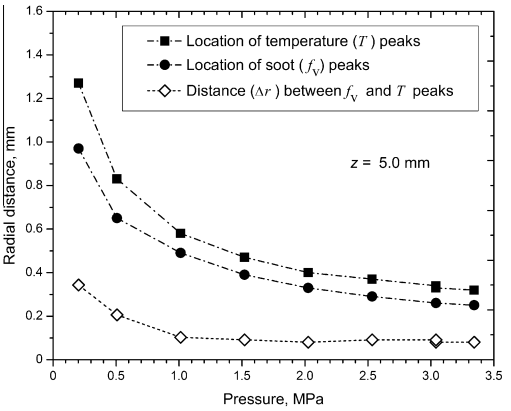

Fig. 4. Variation of the radial locations of the temperature and soot volume fraction peaks as a function of pressure.

height is a better measure than the maximum line-of-sight integrated soot concentrations. We use the same approach here to assess the influence of pressure. The mass flow rate of carbon, in the form of soot, can be determined through the relationship

$$\dot{m}_s(z) = v_z(z)\rho_s \int 2\pi r f_v(r,z)\mathrm{d}r,$$

where v_z is the axial velocity, $\rho_s = 1.8$ g/cm^3 is the soot density, and z is the axial height. The axial velocity is estimated using the relationship $v_z(z) = \sqrt{2az}$, where a is an acceleration constant commonly assumed to be 25 m/s^2 [1]. The percentage of carbon in the fuel converted to soot is simply $\eta_s = \dot{m}_s/\dot{m}_c$, where $\dot{m}_c$ is the carbon mass flow rate at the nozzle exit. The results of this calculation are plotted in Fig. 6. Peak carbon conversion occurs at a height of about 6 mm above the burner nozzle at a pressure of 0.2 MPa, 5.0 mm for a pressure of 0.51 MPa, and 4.5 mm for pressures from 1.52 to 3.34 MPa, Fig. 6.

A plot of maximum percentage conversion of carbon to soot as a function of pressure is shown in Fig. 7. However, a power-law relationship that covers the whole pressure range between the percentage conversion of fuel's carbon to soot and the pressure is not obvious. This trend is similar to previous measurements with methane and propane diffusion flames [4–6]. If a power-law relationship is forced, it would be necessary to divide the plot into three separate pressure regions, Fig. 7. Approximate fits to the three sets of data points in the form $\eta_s \propto P^n$ yield $n = 2.2$ for pressures ranging between 0.2 and 0.5 MPa, $n = 1.1$ for the pressure range of 0.5–1.52 MPa, and $n = 0.4$ for the pressure range of 1.52–3.34 MPa. These observations depict that carbon conversion to soot has a decreasing sensitivity to increasing pressure.

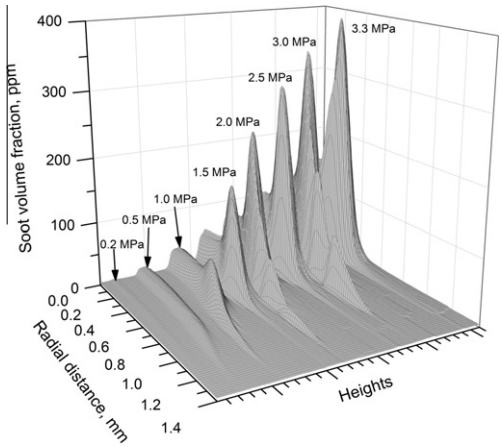

Fig. 5. A three-dimensional rendition of the soot volume fraction as a function of pressure and the spatial location within the flame. It should be noted that the "Heights" axis is a repeating coordinate representing successive height measurement locations from the burner tip for each pressure.

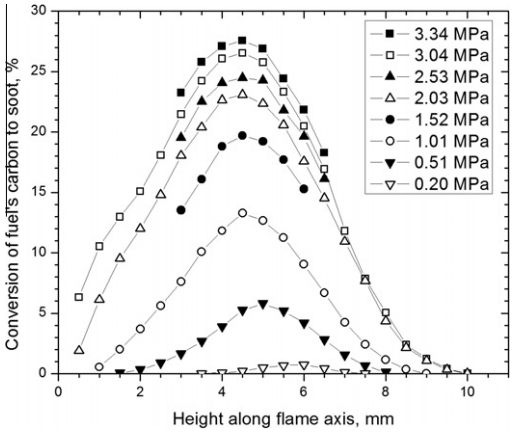

Fig. 6. Percentage conversion of carbon from fuel to soot as a function of axial location along the flame axis.

The pressure exponent $n = 1.1$ obtained for ethane diffusion flames in the range of 0.5–1.52 MPa is very close to $n = 1$ reported for methane flames in the range of 0.5–2 MPa [4]. The same exponent, $n = 1.1$, is reported for propane diffusion flames [6] in the range of 0.2–0.73 MPa. In the current study, the pressure exponent is 0.4 between 1.52 and 3.34 MPa similar to methane flames [5]. It seems that the pressure sensitivity of soot formation experiences a transition around 1.5–2.0 MPa, and it decreases significantly as the pressure is further increased, Fig. 7.

The carbon conversion to soot peaked at about 28% at 3.34 MPa in comparison to about 10% at 3 MPa and about 15% at 6 MPa in methane diffusion flames [5]. The maximum conversion of fuel's carbon to soot is reported as 20% for a propane diffusion flames at 0.73 MPa [6]. The differences are mostly due to the influence of fuel chemical structure on pyrolysis and the subsequent soot formation process.

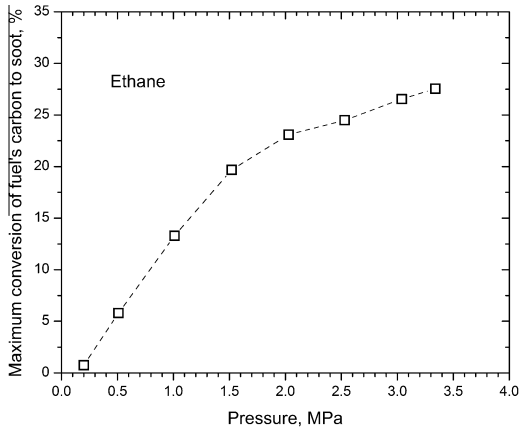

Fig. 7. Maximum percentage conversion of carbon from fuel to soot as a function of pressure.

Results prompt several questions about the causes of the observed trend in soot concentration with pressure. Without detailed chemical kinetic modelling of the diffusion flames investigated in the current work, it would be difficult to pinpoint the causes of the presented results. It is recognized that increased pressure has a non-trivial effect on gas-phase chemistry through enhancing the rate of reactions that are weakly dependent on temperature and through pressure-dependent third-body reactions [15,16]. The kinetics of pressure dependence have been explored extensively, and most such studies focus on the competition between two particularly important reactions that influence the chain properties of the hydrocarbon mechanism. For laminar flame propagation, the variation of burning velocity with pressure can be related to the fact that the $H + O_2 + M = HO_2 + M$ reaction is pressure dependent. This reaction begins to influence burning rate in the same pressure range as in this study where the pressure dependence was observed to change. This suggests that radical consumption, which is generally pressure dependent, steadily continues as pressure increases, and the soot precursors increasingly have no alternative but to produce more soot as pressure increases. In a numerical simulation effort for similar methane diffusion flames with detailed gas-phase chemistry, Liu et al. [15] show that acetylene concentrations decrease significantly, by about a factor of four, with respect to pressure from 0.5 to 4 MPa. Similar behaviour is observed for OH concentrations [15]. For flames at atmospheric pressure, acetylene

is considered one of the species that plays an important role in soot inception and growth. However, the role of acetylene may not have the same influence on soot formation at elevated pressures. The decrease in OH concentrations with pressure is expected to slow down the oxidation of soot precursors within the soot nucleation region leading to higher nucleation rates. The observed trends seem to be a combined effect of issues discussed above as well as the increased pyrolysis rate of the fuel with pressure and temperature of the flame, which will be discussed in the next subsection.

3.3. Soot temperatures

Averaged temperatures from line-of-sight emission measurements through the flame centerline as a function of height along flame axis at various pressures are shown in Fig. 8. It should be noted that the temperatures plotted in Fig. 8 represent a soot concentration-weighted average temperature along a chord through the flame centerline (perpendicular to the flame axis). Therefore, these temperatures should correspond closely to peak soot volume fraction location temperatures [13].

A high temperature region is observed close to the flame base similar to data reported in [4,17]. One of the reasons for this is the preheating of the reactants by the fuel nozzle, which is at a higher temperature as a result of heat transfer from the flame. It is clear that the average temperatures generally decrease with pressure as a result of increasing heat loss by radiation from the flame, Fig. 8.

The rate of temperature increase with axial position increases with increasing pressure; however, the overall temperature drops with increasing pressure, most significantly in the lower half of the flame. As the pressure increases, the visible flame gets narrower resulting in steeper radial temperature gradients. Maximum radial temperature gradients, calculated from the temperature profiles, are shown in Fig. 9. The gradients are highest near the burner rim, and generally decrease with increasing height. The radial temperature gradients generally increase with pressure at very low heights and near the tip of the flame. At heights in between, the gradients reach a plateau at around 1.5 MPa and then decrease as the pressure is further increased. Near the burner nozzle, radial temperature gradients are as high as 2000 K/mm at the higher pressures, whereas they drop to about zero near the tip of the flame, Fig. 9. Higher radial temperature gradients near the burner exit at higher pressures mean that the thermal diffusion from the hot regions of the flame towards the flame centerline is enhanced. This causes higher fuel pyrolysis rates which lead to accelerated soot nucleation and growth as the pressure increases. A complete account of the detailed temperature data is given in [4–6,18].

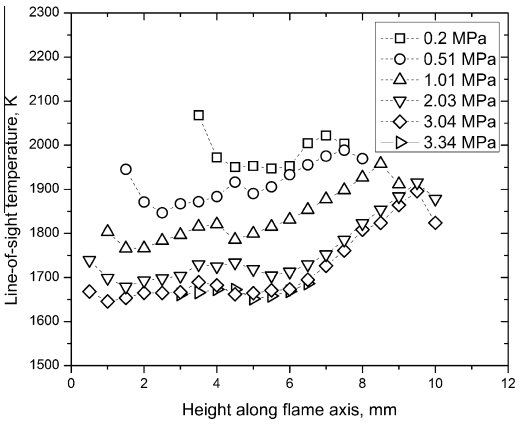

Fig. 8. Line-of-sight emission averaged soot temperature along the flame axis as a function of flame axial locations at various pressures.

3.4. Measurement uncertainties

Some degree of uncertainty is introduced to the measured temperature and soot volume fractions due to a lack of understanding of the dependence of soot optical properties, specifically soot refractive index and consequently the refractive index absorbtion function $E(m)$, on soot temperature, soot aggregate structure, and wavelength. The results of a limited number of studies on the dependence of refractive index on soot temperature reveal that at typical flame temperatures the dependence is not significant. However, from room temperature to flame temperatures the imaginary part of the refractive index may change by 50% [19,20]. A recent comprehensive review [21] shows that Rayleigh-Debye-Gans polydisperse fractal aggregate approach can properly describe the light scattering from soot aggregates as long as the aggregate fractal dimension is less 2. This approach assumes that the absorbtion coefficient of soot does not depend on the extent of aggregation, and there is good evidence that the fractal dimension of soot aggregates is about 1.8 [22–24]. We assumed, for the purposes of this work and to be consistent with the previous high-pressure soot measurements [4,6], that the soot refractive index does not have a significant dependence on temperature or on aggregate size.

Another source of uncertainty originates from the dependence of the function $E(m)$ on wavelength. Based on the previous analysis and estimates [13,25] a constant $E(m)$ function with a magnitude of 0.274 is assumed in the present work. This is consistent with the results of Krishnan et al. [25] and the previous measurements with methane [4,5] and propane flames [6].

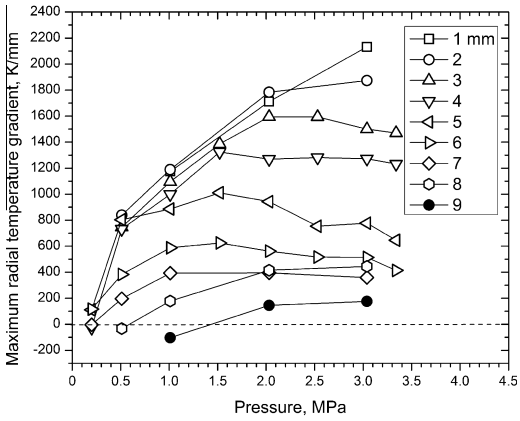

Fig. 9. Maximum radial gradients of soot temperature along the flame axis as a function of pressure at various flame axial locations.

Modelling of the flame emission using the methods described in [13] showed that attenuation of emission by soot introduces only a small error in the measurements (i.e., <2%) for even the highest soot loadings observed in this flame. This result may seem surprising considering that soot volume fractions of 375 ppm have been measured in this flame; however, light attenuation is a function of the product of the soot concentration and the absorption path length. Although soot concentrations are a factor of ten larger than those observed in the familiar atmospheric flames, e.g., [26,27], the flame diameter is much smaller and decreases with increasing pressure. A more detailed discussion of the subject can be found in [28].

Reliable measurements using the SSE method were only possible in radial regions around the emission intensity annulus as noted before [4–6]. The total uncertainty of the temperature and soot volume fraction measurements is dominated by the uncertainty of the soot refractive index as discussed above. The total uncertainty in temperature was estimated as 3.5% and the total uncertainty in soot volume fraction as 30% with a 95% confidence interval at 0.2 MPa; at higher pressures the total uncertainty was evaluated as less than 8% [4–6,18].

4. Conclusions

Soot volume fraction and soot temperature profiles were measured using spectral soot emission to study the sensitivity of soot formation to pressure in co-flow laminar diffusion flames of ethane in air in a high pressure combustion vessel. The range of pressures investigated was from 0.2 to 3.34 MPa. The mass flow rate of ethane was kept constant at all pressures. Visible flame heights, as indicated by soot radiation, remained constant at about 10 mm between 1.01 and 3.34 MPa. For pressures lower than 1.01 MPa, visible flame heights decreased with decreasing pressure. Between 0.2 and 3.34 MPa, the cross-sectional area of the flame (measured from the radius defined by either the maximum soot or maximum temperature annuli) showed an inverse dependence on pressure. Peak carbon conversion to soot, defined as the percentage of the fuel's carbon content converted to soot, followed a power-law dependence on pressure, where the pressure exponent was about 2.2 for pressures between 0.2 and 0.51 MPa, 1.1 for 0.51–1.52 MPa, and 0.4 for 1.52–3.34 MPa. These exponents are comparable to the exponents reported for methane diffusion flames in similar pressure ranges. The maximum conversion of the fuel's carbon to soot, 28%, was observed at 3.34 MPa at approximately the mid height of the flame. Averaged flame temperatures decreased with increasing pressure as a result of enhanced heat loss from the flame by soot radiation.

Acknowledgments

We acknowledge an infrastructure grant provided by Canadian Foundation for Innovation. Operational funds for this work have been provided by Natural Sciences and Engineering Research Council and Canadian Space Agency.

References

[1] W.L. Flower, C.T. Bowman, *Proc. Combust. Inst.* 21 (1988) 1115–1124.
[2] W. Lee, Y.D. Na, *JSME Int. J. Ser. B* 43 (4) (2000) 550–555.
[3] L.L. McCrain, W.L. Roberts, *Combust. Flame* 140 (2005) 60–69.
[4] K.A. Thomson, Ö.L. Gülder, E.J. Weckman, R.A. Fraser, G.J. Smallwood, D.R. Snelling, *Combust. Flame* 140 (2005) 222–232.
[5] I.H. Joo, Ö.L. Gülder, *Proc. Combust. Inst.* 32 (2009) 769–775.
[6] D.S. Bento, K.A. Thomson, Ö.L. Gülder, *Combust. Flame* 145 (2006) 765–778.
[7] A.S. Bodke, D.A. Olschki, L.D. Schmidt, E. Ranzi, *Science* 285 (1999) 712–715.
[8] G.F. Glasier, P.D. Pacey, *Carbon* 39 (2001) 15–23.
[9] Anon., *Chem. Eng. News* 84 (28) (2006) 59–68.
[10] H. Gohari Darabkhani, J. Bassi, H.W. Huang, Y. Zhang, *Fuel* 88 (2009) 264–271.
[11] C.H. Kim, F. Xu, G.M. Faeth, *Combust. Flame* 152 (2008) 301–316.
[12] P.M. Mandatori, Ö.L. Gülder, *Combust. Flame* 150 (2007) 400–403.
[13] D.R. Snelling, K.A. Thomson, G.J. Smallwood, Ö.L. Gülder, E.J. Weckman, R.A. Fraser, *AIAA J.* 40 (9) (2002) 1789–1795.
[14] C.J. Dasch, *Appl. Opt.* 31 (8) (1992) 1146–1152.
[15] F. Liu, K.A. Thomson, H. Guo, G.J. Smallwood, *Combust. Flame* 146 (2006) 456–471.

[16] J. Warnatz, U. Maas, R.W. Dibble, *Combustion*, 4th ed., Springer Verlag, Heidelberg, 2006, p. 81.
[17] W.L. Flower, *Combust. Flame* 77 (1989) 279–293.
[18] P.M. Mandatori, MASc. thesis, Institute for Aerospace Studies, University of Toronto, Canada, 2006.
[19] S.C. Li, C.L. Tien, *Proc. Combust. Inst.* 18 (1981) 1159–1166.
[20] T.T. Charalampopoulos, H. Chang, B. Stagg, *Fuel* 68 (1989) 1173–1179.
[21] C.M. Sorenson, *Aerosol Sci. Technol.* 35 (2) (2001) 648–687.
[22] T.L. Farias, M.G. Carvalho, Ö.Ü. Köylü, G.M. Faeth, *J. Heat Transfer* 117 (1) (1995) 152–159.
[23] G.M. Faeth, Ö.Ü. Köylü, *Combust. Sci. Technol.* 108 (4–6) (1995) 207–229.
[24] T.L. Farias, Ö.Ü. Köylü, M.G. Carvalho, *Appl. Opt.* 35 (33) (1996) 6560–6567.
[25] S.S. Krishnan, K.-C. Lin, G.M. Faeth, *J. Heat Transfer* 122 (2000) 517–524.
[26] D.R. Snelling, K.A. Thomson, G.J. Smallwood, Ö.L. Gülder, *Appl. Opt.* 38 (12) (1999) 2478–2485.
[27] R.J. Santoro, T.T. Yeh, J.J. Horvath, H.G. Semerjian, *Combust. Sci. Technol.* 53 (2–3) (1987) 89–115.
[28] J.J. Murphy, C.R. Shaddix, *Combust. Flame* 143 (2005) 1–10.